AIAA JOURNAL
Vol. 34, No. 9, September 1996

Hybrid Computational Model for Noise Propagation Through a Fuselage Boundary Layer

Harmen Schippers*
National Aerospace Laboratory NLR, 8300 AD Emmeloord, The Netherlands
and
Jeroen A. Wensing†
University of Twente, 7500 AE Enschede, The Netherlands

A hybrid computational model is presented to predict scattering and refractive effects on acoustic waves propagating through a boundary layer surrounding an aircraft fuselage. The fuselage is represented by an infinitely long cylinder with a noncircular cross section. The propagation effects through the boundary layer can be significant and should be included in noise predictions. The computational model uses finite elements to solve the acoustic pressure inside the boundary-layer area and boundary elements to calculate the pressure outside the boundary layer. An important advantage of the present model is that complicated geometries can be handled more easily than with prediction models that are based on analytical techniques. Most of these analytical prediction models are limited to circular cross shapes of fuselages. The purpose of the present investigation is to overcome this limitation and to assess the effects of noncircular geometries by comparing the pressure distributions with those of circular geometries. The computational model is applied to the noncircular cross section of a Fokker 50-like fuselage.

Nomenclature

c	= speed of sound
G	= Green's function
$H_0^{(2)}$	= zeroth-order Hankel function of the second kind
i	= unit vector in x direction
K, V	= boundary integral operators
k	= wave number source
k_t	= transverse wave number source
k_x	= axial wave number source
M	= axial Mach number of mean flow
N_i^0	= constant shape functions
N_i^1	= linear shape functions
P	= pressure (y, z)
p	= pressure (x, y, z, t)
R	= radius of cylinder
r	= radial coordinate function of y and z
$\boldsymbol{r}, \boldsymbol{r}'$	= position vector (y, z)
r_p, θ_p	= polar coordinates
S	= edge of boundary-layer area
t	= time
U	= axial component of mean flow
v	= velocity of mean flow
W	= test function
x, y, z	= Cartesian coordinates
α	= axial wave number
γ	= wave number Helmholtz equation
δ	= boundary-layer thickness
ρ	= density, normalized boundary-layer coordinate
ϕ_i	= angle of incidence
ϕ_v	= visual angle of incidence
ψ	= test function
ω	= frequency

Subscripts

e	= interface boundary
i	= fuselage boundary
0	= mean flow
1	= boundary-layer area
2	= region outside boundary-layer area

Superscripts

e	= element
i	= incident field
s	= scattered field

Received June 12, 1995; revision received Nov. 6, 1995; accepted for publication Nov. 16, 1995.

*Senior Research Engineer, Theoretical Aerodynamics Department, P.O. Box 153.
†Ph.D. Student, Department of Mechanical Engineering.

Introduction

INVESTIGATIONS of the acoustic field around the fuselage of a propeller-driven aircraft are motivated by the urge to reduce cabin noise. Knowledge of the sound pressure on the outer fuselage surface is necessary to predict the noise inside the cabin. This pressure is not just the sound pressure of an isolated propeller on the same relative locations because this free field pressure is affected by the presence of the fuselage itself and its boundary layer. The propagation effects through the boundary layer can be significant and should be included in the noise predictions.

The scattering of sound by the fuselage can be described by classical diffraction theory, extended for the presence of a main flow.[1] The analysis of the influence of the boundary layer involves a theoretical description of the refraction of sound by a nonuniform shear flow. The effects of this flowfield on the acoustic pressure at the outer fuselage surface have been investigated by several other authors.[2–5] These investigations were limited to circular cross shapes of fuselages. The purpose of this paper is to overcome this limitation by presenting a computational model that can also be applied to noncircular cross shapes.

The computational model uses finite elements to solve the acoustic pressure inside the boundary layer and boundary elements to calculate the pressure outside the boundary layer. The solution in the boundary layer and the solution outside the boundary layer are coupled by requiring the pressure and its gradient to be continuous at the interface of both areas. This coupling procedure has been discussed by Costabel et al.[6] An important advantage of the present hybrid computational model is that complicated geometries can be handled more easily than with prediction models that are based on analytical techniques. An example of a slightly more complicated geometry is a cross section similar to the Fokker 50 fuselage (Fig. 1).

The objectives of the present investigation are to establish the applicability of the computational model to predict the acoustic

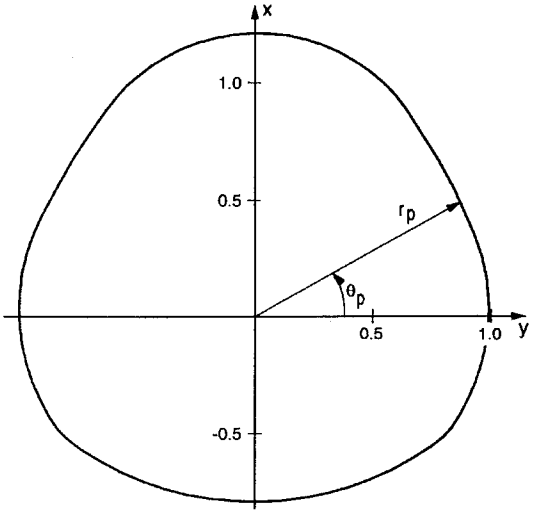

Fig. 1 Geometry of a cross section similar to a Fokker 50-like fuselage.

effects of a fuselage boundary layer on the noise propagation, to discuss the modeling of the shear flow, and to assess the effects of the noncircular cross shape of a Fokker 50-like fuselage by comparing the pressure distributions with those of a circular geometry.

Theoretical Formulation

The fuselage of an aircraft is modeled by an infinitely long cylinder with a noncircular cross section, ranging from $x = -\infty$ to $+\infty$. In the present investigations only the effects of velocity gradients are considered. The effects of gradients in thermodynamic variables are neglected. Then, the solution of the Euler equations is given by a unidirectional cylindrically sheared mean flow with

$$v_0 = iU[r(y, z)], \qquad \rho_0 = \text{const}, \qquad p_0 = \text{const} \tag{1}$$

where i denotes the unit vector in the direction of the flow. The coordinate variable r is an arbitrary function of the coordinates y and z, defining the cross-sectional plane. The surfaces $r = \text{const}$ are coordinate surfaces in a cylindrical coordinate system where the mean velocity $U(r)$ remains constant. Changes in U occur only in the direction normal to these surfaces. Outside the boundary layer we have a uniform flow in the positive x direction with constant velocity, i.e., $U(r) = U_0$ for $r > R + \delta$. Inside the boundary layer, i.e., $R < r < R + \delta$, the mean velocity $U(r)$ is a function of the coordinate r.

The governing equation for the acoustic pressure field follows from linearizing the Euler equations about the mean steady flow given by Eq. (1). As has been derived by Goldstein,[7] it reads

$$\frac{\mathrm{D}}{\mathrm{D}t}\left(\Delta p - \frac{1}{c_0^2}\frac{\mathrm{D}^2 p}{\mathrm{D}t^2}\right) - 2\frac{\mathrm{d}U(r)}{\mathrm{d}r}\frac{\partial^2 p}{\partial r \partial x} = 0 \tag{2}$$

with the substantial derivative

$$\frac{\mathrm{D}}{\mathrm{D}t} = \frac{\partial}{\partial t} + U(r)\frac{\partial}{\partial x} \tag{3}$$

Furthermore, c_0 is the speed of sound of the mean flow and

$$\frac{\partial}{\partial r} = \frac{\nabla r}{|\nabla r|^2} \cdot \nabla \tag{4}$$

The waves are assumed to propagate harmonically in time with frequency ω and with wave number α in axial direction, i.e.,

$$p(t, x, y, z) = P(y, z)e^{i(\omega t + \alpha x)} \tag{5}$$

When Eq. (5) is substituted into Eq. (2) the equation for P becomes

$$[\Delta + \gamma^2(r)]P - F(r)\frac{\partial P}{\partial r} = 0 \tag{6}$$

with

$$\gamma(r) = \sqrt{\{k + [1 + M(r)]\alpha\}}\sqrt{\{k - [1 - M(r)]\alpha\}} \tag{7}$$

and

$$F(r) = \frac{2\alpha}{[k + M(r)\alpha]}\frac{\mathrm{d}M(r)}{\mathrm{d}r} \tag{8}$$

Furthermore, $M(r)$ is the Mach number [i.e., $M(r) = U(r)/c$] and $k = \omega/c$. Outside the boundary layer Eq. (6) reduces to

$$\left(\Delta + \gamma_0^2\right)P = 0 \tag{9}$$

with

$$\gamma_0 = \sqrt{[k + (1 + M_0)\alpha]}\sqrt{[k - (1 - M_0)\alpha]} \tag{10}$$

The total pressure field consists of an incoming and a scattered field, i.e.,

$$P(y, z) = P^s(y, z) + P^i(y, z) \tag{11}$$

Equations (6) and (9) are to be solved under the following boundary conditions:

1) P^s should consist of outgoing waves.

2) The normal component of the particle velocity on the fuselage boundary vanishes, i.e.,

$$\frac{\partial P}{\partial n} = 0 \tag{12}$$

3) The acoustic pressure and its normal derivative are continuous at the edge of the boundary layer for $r = R + \delta$.

Coupled Mathematical Formulation

Equation (6) is solved in a weak sense. Let the boundary-layer area be given by A_1 with boundaries S_i and S_e, where S_i corresponds with the surface of the fuselage and S_e with the edge of the boundary layer. By the divergence theorem of Gauss, it follows from Eq. (6) that the acoustic pressure field P_1 inside A_1 has to satisfy

$$\iint_{A_1}\left[\nabla W \cdot \nabla P_1 - W\gamma^2(r)P_1 + WF(r)\frac{\partial P_1}{\partial r}\right]\mathrm{d}A - \int_{S_e}\frac{\partial P_1}{\partial n}W\,\mathrm{d}s - \int_{S_i}\frac{\partial P_1}{\partial n}W\,\mathrm{d}s = 0 \tag{13}$$

for all test functions W.

The boundary integral over S_i vanishes because of condition (12). Equation (13) is briefly written as

$$a(P_1, W) - \left\langle\frac{\partial P_1}{\partial n}, W\right\rangle = 0 \tag{14}$$

where a is a functional representing the first term of Eq. (13) and $\langle,\rangle$ is an inner product over boundary S_e.

Outside the boundary layer, the pressure satisfies the Helmholtz equation (9) with a constant wave number. Here the scattered pressure is given by the boundary integral representation formula

$$P_2^s(\boldsymbol{r}) = \int_{S_e}\frac{\partial P_2^s(\boldsymbol{r}')}{\partial n}G(\boldsymbol{r}, \boldsymbol{r}')\,\mathrm{d}s_{r'} - \int_{S_e}P_2^s(\boldsymbol{r}')\frac{\partial}{\partial n_{r'}}G(\boldsymbol{r}, \boldsymbol{r}')\,\mathrm{d}s_{r'}, \qquad \boldsymbol{r} \notin S_e \tag{15}$$

The fundamental solution G of the two-dimensional Helmholtz equation is given by

$$G(\boldsymbol{r}, \boldsymbol{r}') = (i/4)H_0^{(2)}(\gamma_0|\boldsymbol{r} - \boldsymbol{r}'|) \tag{16}$$

Whenever $\boldsymbol{r}$ is part of boundary S_e, the second integral of Eq. (15) becomes singular. By the jump relations of classical potential theory, it follows that

$$\frac{1}{2}P_2^s(\boldsymbol{r}) = \int_{S_e} \frac{\partial P_2^s(\boldsymbol{r}')}{\partial n} G(\boldsymbol{r}, \boldsymbol{r}')\, \mathrm{d}s_{r'} - \int_{S_e} P_2^s(\boldsymbol{r}') \frac{\partial}{\partial n_{r'}} G(\boldsymbol{r}, \boldsymbol{r}')\, \mathrm{d}s_{r'}, \qquad \boldsymbol{r} \in S_e \tag{17}$$

where the second integral in Eq. (17) exists as an improper integral. The boundary integral equation (17) has a unique solution,[8] except at resonance frequencies of the interior acoustic problem related to boundary S_e. Equation (17) is also solved in a weak sense. For arbitrary functions ψ, we require that

$$\int_{S_e} \frac{1}{2} P_2^s(\boldsymbol{r}) \psi \, \mathrm{d}s - \int_{S_e}\int_{S_e} \frac{\partial P_2^s(\boldsymbol{r}')}{\partial n} G(\boldsymbol{r}, \boldsymbol{r}')\, \mathrm{d}s_{r'} \psi(\boldsymbol{r})\, \mathrm{d}s_r + \int_{S_e}\int_{S_e} P_2^s(\boldsymbol{r}') \frac{\partial}{\partial n_{r'}} G(\boldsymbol{r}, \boldsymbol{r}')\, \mathrm{d}s_{r'} \psi(\boldsymbol{r})\, \mathrm{d}s_r = 0 \tag{18}$$

which is briefly written as

$$\left\langle \frac{1}{2} P_2^s, \psi \right\rangle - \left\langle V \frac{\partial P_2^s}{\partial n}, \psi \right\rangle + \left\langle K P_2^s, \psi \right\rangle = 0 \tag{19}$$

The integral operators V and K correspond to potentials as a result of single layer and double layer distributions on the boundary S_e.

The coupled mathematical formulation is obtained by means of the pressure field continuity equations on the interface boundary S_e:

$$\frac{\partial P_1}{\partial n} = \frac{\partial P_2}{\partial n} \qquad P_1 = P_2 = P_2^s + P_2^i \tag{20}$$

When these continuity equations are substituted into Eqs. (14) and (19), the coupled problem to be solved reads: find the pressure P_1 and its normal derivative at boundary S_e,

$$\mu = \left.\frac{\partial P_1}{\partial n}\right|_{S_e} = \left.\frac{\partial P_2}{\partial n}\right|_{S_e} \tag{21}$$

such that

$$a(P_1, W) - \langle \mu, W \rangle = 0 \tag{22}$$

and

$$\left\langle \frac{1}{2} P_1, \psi \right\rangle - \langle V\mu, \psi \rangle + \langle K P_1, \psi \rangle = \left\langle \frac{1}{2} P_2^i, \psi \right\rangle - \left\langle V \frac{\partial P_2^i}{\partial n}, \psi \right\rangle + \left\langle K P_2^i, \psi \right\rangle \tag{23}$$

for all test functions W and ψ. This coupling procedure has been described for Laplace's equation by Costabel et al.[6]

Hybrid Computational Model

The coupled mathematical formulation (22) and (23) is numerically solved by a combination of finite elements and boundary elements. The pressure field P_1 in the inner region A_1 is discretized using a finite element formulation. Therefore, the inner area A_1 is divided into triangular elements. An example of a triangular mesh around a Fokker 50-like fuselage is presented in Fig. 2, where the thickness of the boundary layer has been blown up ease of visualization. The pressure in A_1 is approximated by piecewise linear local shape functions. For each element e, it follows that

$$P_1^e(y, z) = \sum_{i=1}^{3} P_{1i}^e N_i^1(y, z) \tag{24}$$

where $N_i^1(y, z)$ are the piecewise linear shape functions. The unknowns are the values of the pressure in the nodes of the triangular mesh. According to Galerkin's method, the test functions W are chosen to correspond with the local linear shape functions N_i^1. The

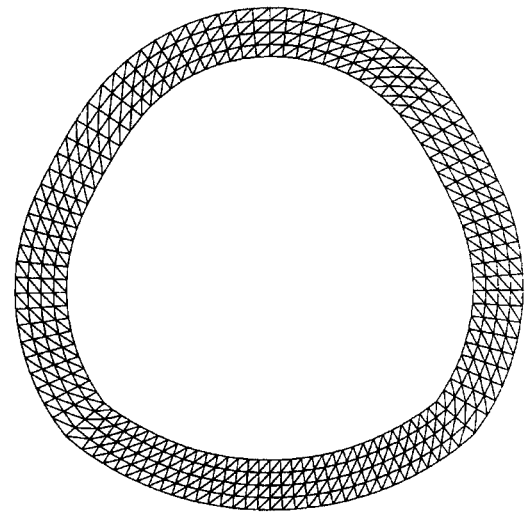

Fig. 2 Example of a computational grid around a Fokker 50-like fuselage.

remaining integrals of the first part of Eq. (22) are calculated with a second-order Gaussian quadrature rule with four weight points.

The pressure on the boundary S_e and its normal derivative are discretized using boundary elements. The boundary element mesh on S_e coincides with the outer boundary of the finite element mesh covering the inner area. The pressure is approximated by piecewise linear shape functions analogous to the pressure in the inner area and, as a consequence, the normal derivative of the pressure is approximated by piecewise constant shape functions. It follows that

$$P_1^e(\boldsymbol{r}) = \sum_{i=1}^{2} P_{1i}^e N_i^1(\boldsymbol{r}) \quad \text{and} \quad \frac{\partial P_1^e(\boldsymbol{r})}{\partial n} = \frac{\partial P_1^e}{\partial n} N^0, \qquad \boldsymbol{r} \in S_e \tag{25}$$

The local linear shape functions $N_i^1(\boldsymbol{r})$ are associated with each corner node. They are equal to one for the node with which they are associated and zero for the other node of element e. The local constant shape functions N^0 are equal to one over the whole element e. According to Galerkin's method the test functions W and ψ are chosen to correspond with the local shape functions:

$$W^e(\boldsymbol{r}) = N_i^1(\boldsymbol{r}) \quad \text{and} \quad \psi^e = N^0, \qquad i = 1, 2 \tag{26}$$

The approximations (25) and (26) are substituted into the boundary integrals of the inner products of Eqs. (22) and (23). The remaining integrals are again calculated with Gaussian quadrature rules, i.e., a fourth-order rule for the inner integral occurring in the boundary operators K and V and a second-order rule for the outer integrals. An exception is made for the boundary element part resulting from V, when the contribution of an element to itself has to be determined. For this case the operator V yields a weakly singular integral that is calculated analytically where the Hankel function of Eq. (16) is represented by a mathematical series for small arguments. Details of the calculation of the boundary integrals have been given by Wensing.[9]

When the outlined numerical approach is followed, the coupled mathematical formulation (22) and (23) yields the hybrid computational model. The final system of equations reads

$$\begin{bmatrix} A & B \\ C & D \end{bmatrix} \begin{bmatrix} X_1 \\ X_2 \end{bmatrix} = \begin{bmatrix} 0 \\ F_2 \end{bmatrix} \tag{27}$$

The vector $\boldsymbol{X}_1$ consists of the values of the discretized pressure in the boundary-layer area A_1 and at the boundary S_e. Submatrix A is the finite element part related to the approximation of the functional a in Eq. (22). The matrix A has a banded structure because local shape functions are used to approximate the pressure. The bandwidth of the matrix A depends strongly on the numbering of the nodes of

the triangular mesh. The bandwidth can be minimized using a suitable reordering algorithm. In the present computational model the Gibbs–King algorithm has been applied.[10] The vector X_2 consists of the discretized normal derivative of the pressure on boundary S_e. Submatrix D follows from the boundary element approximation of $\langle V\mu, \psi\rangle$. The matrix D is a full symmetric matrix because of the symmetry of the boundary integral operator V. Matrices B and C, which are sparsely filled, are the coupling parts. They correspond with the approximation of $\langle \mu, W\rangle$ and $\langle \frac{1}{2}(I + K)P_1, \psi\rangle$, respectively. The right hand side vector F_2 is determined by the prescribed incident field, i.e., the right-hand side of Eq. (23).

The system of equations (27) is solved by block Gauss decomposition using a skyline solver for matrix A. The computational model has been implemented on NLR's NEC SX3 supercomputer. For a finite element mesh consisting of 1440 triangles and a boundary element mesh of 160 segments the computation time amounts 55 CPU s, where about 80% of the computation time is required for the evaluation of the boundary elements matrices C and D of Eq. (27). For the case of Laplace's equation the convergence of the hybrid computational model was investigated by Costabel et al.[6] By mathematical analysis it was proven that the model should converge to second order when the mesh is uniformly refined. This was experimentally established by numerical experiments. The second-order convergence has also been observed by the authors,[9,11] who applied the hybrid model (27) to solve the Helmholtz equation [corresponding to the case $M(r) = 0$ in Eq. (6)] around a cylinder with circular cross section for $kR = 10$. The calculated values of the pressure at the boundary of the cylinder were compared with the analytical solution. It has been observed that the convergence rate of the L_2 error of the pressure at boundary S_i is approximately two, when the mesh size of the computational grid is refined uniformly.

Modeling of Boundary-Layer Shear Flow

The modeling of the shear flow is investigated for the case of a cylinder with a circular cross section with radius $R = 1$ and boundary-layer thickness $\delta = 0.025$. The incoming acoustic wave is prescribed by a plane wave (unit strength), which has components in both axial and transverse direction, given by

$$p(x, y, z, t) = e^{i\omega t}e^{-i(k_x x - k_t y)} \tag{28}$$

with $k_t > 0$. Taking into account Eq. (5), it follows that $\alpha = -k_x$. In the cross section plane it is assumed that the plane wave is incident from the right side (see Fig. 1). The incident wave has to satisfy Eq. (9), so that $k_t = \gamma_0$. From Eq. (10) it can be deduced that

$$(k - M_0 k_x)^2 - \left(k_x^2 + k_t^2\right) = 0 \tag{29}$$

The angle of incidence with respect to the flow is given by

$$\phi_i = \arctan(k_t/k_x) \tag{30}$$

It is assumed that the position of the source is stationary with respect to the cylinder. Because of the nonzero velocity of the mean flow, ϕ_i is not equal to the visual angle ϕ_v, i.e., the angle under which an observer on the cylinder sees the source. The visual angles ϕ_v and ϕ_i are related by

$$\phi_i = \phi_v + \arcsin[M_0 \sin(\phi_v)] \tag{31}$$

Note that $\phi_v = 0$ deg corresponds to a wave propagating in the positive x direction. Whenever ϕ_v and M_0 are prescribed, the value of ϕ_i follows from Eq. (31). The actual values of the axial wave number α and the transverse wave number γ_0 follow from solving k_x and k_t from Eqs. (29) and (30), substituting the value of ϕ_i and taking $\alpha = -k_x$ and $\gamma_0 = k_t$.

Let the normalized boundary layer coordinate in radial direction be given by $\rho = (r - R)/\delta$. For the modeling of the shear flow in the boundary layer, the following velocity profiles are considered: 1) a turbulent velocity profile according to the $\frac{1}{7}$ power law, i.e.,

$$M(\rho) = M_0 \rho^{\frac{1}{7}} \tag{32}$$

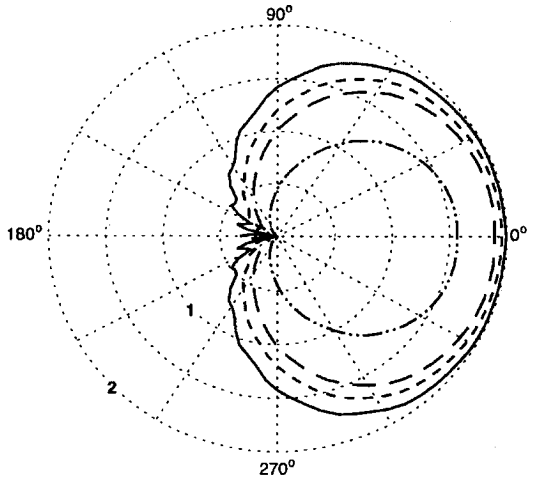

Fig. 3 Effect of different velocity profiles in the boundary layer on the pressure distribution (amplitude) around a cylinder with circular cross section; $k = 5.6$, $M_0 = 0.8$, $\phi_v = 90$ deg: ——, without boundary layer; - - - -, with boundary layer (turbulent velocity profile); – – –, with boundary layer (linear velocity profile based on the same displacement thickness); and ·–·–·–·, with boundary layer (linear velocity profile).

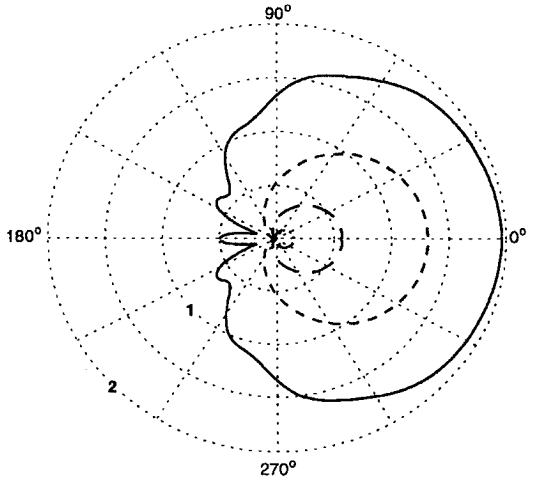

Fig. 4 Effect of different velocity profiles in the boundary layer on the pressure distribution (amplitude) around a cylinder with circular cross section; $k = 5.6$, $M_0 = 0.8$, $\phi_v = 135$ deg: ——, without boundary layer; - - - -, with boundary layer (turbulent velocity profile); – – –, with boundary layer (linear velocity profile based on the same displacement thickness); and ·–·–·–·, with boundary layer (linear velocity profile).

2) a linear velocity profile given by $M(\rho) = M_0\rho$, and 3) a piecewise linear velocity profile approximating the $\frac{1}{7}$ power law that is based on the same displacement thickness,[12] i.e.,

$$\begin{aligned} M(\rho) &= M_0\rho/\delta^*, \qquad 0 < \rho < \delta^* \\ &= M_0, \qquad \rho > \delta^* \end{aligned} \tag{33}$$

with δ^* twice the displacement thickness of Eq. (32). It can be deduced that $\delta^* = \delta/4$.

For $M_0 = 0.8$ and $k = 5.6$, results of the hybrid computational method are given in Figs. 3–5 for three different visual angles of incidence. In these figures the amplitude of the acoustic pressure on the cylinder is plotted for values of the polar angle θ. The results reveal that the shape of the velocity profile in the boundary layer has a large effect on the acoustic pressure on the cylinder, in particular for $\phi_v > 90$ deg. The linear velocity profile and the shear layer model (33) based on the same displacement thickness appear not to be a good approximation for the turbulent velocity profile. This can be explained by the fact that waves do not propagate through the entire boundary layer. They propagate until the cutoff point, where the wave number turns complex. It can be shown that the cutoff point according to Eq. (32) is closer to the fuselage surface

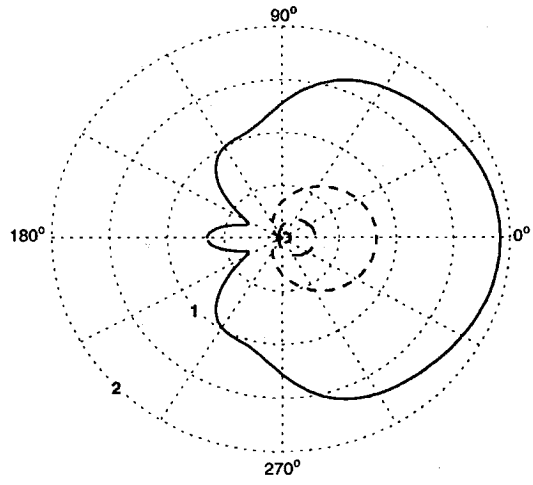

Fig. 5 Effect of different velocity profiles in the boundary layer on the pressure distribution (amplitude) around a cylinder with circular cross section; $k = 5.6$, $M_0 = 0.8$, $\phi_v = 153$ deg: ——, without boundary layer; - - - -, with boundary layer (turbulent velocity profile); – – –, with boundary layer (linear velocity profile based on the same displacement thickness); and ·—·—·, with boundary layer (linear velocity profile).

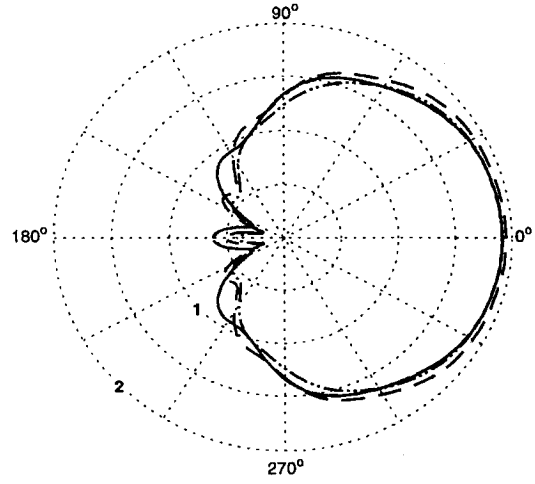

Fig. 6 Effects of Mach number and boundary-layer flow on the pressure distribution (amplitude) around a cylinder with circular cross section; $k = 2.8$, $\phi_v = 90$ deg: ——, no boundary layer (Mach = 0.4); - - - -, turbulent velocity profile (Mach = 0.4); – – –, no boundary layer (Mach = 0.8); and ·—·—·, turbulent velocity profile (Mach = 0.8).

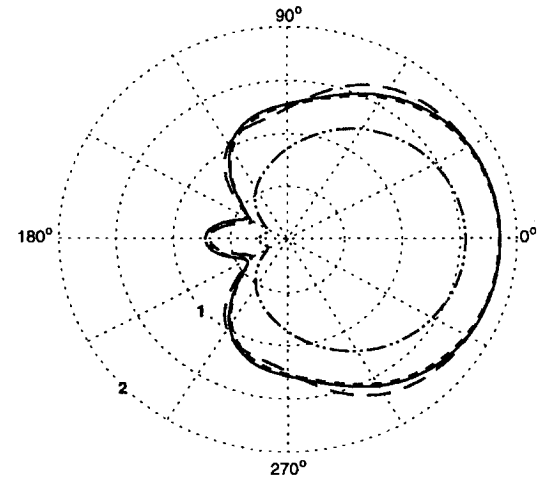

Fig. 7 Effects of Mach number and boundary-layer flow on the pressure distribution (amplitude) around a cylinder with circular cross section; $k = 2.8$, $\phi_v = 135$ deg: ——, no boundary layer (Mach = 0.4); - - - -, turbulent velocity profile (Mach = 0.4); – – –, no boundary layer (Mach = 0.8); and ·—·—·, turbulent velocity profile (Mach = 0.8).

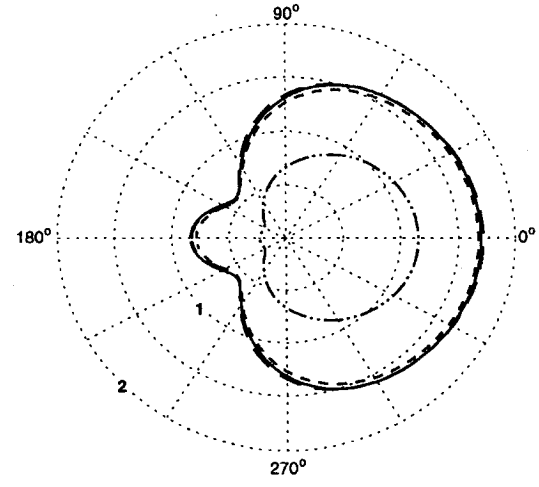

Fig. 8 Effects of Mach number and boundary-layer flow on the pressure distribution (amplitude) around a cylinder with circular cross section; $k = 2.8$, $\phi_v = 153$ deg: ——, no boundary layer (Mach = 0.4); - - - -, turbulent velocity profile (Mach = 0.4); – – –, no boundary layer (Mach = 0.8); and ·—·—·, turbulent velocity profile (Mach = 0.8).

than the cutoff point as follows from Eq. (33). From these results it is concluded that the boundary-layer velocity profile should be described as accurately as possible. This conclusion is found to fit the results of Spence.[5]

Effects of Mach Number and Angle of Incidence

The effects of the boundary-layer shear flow on the resultant noise strongly depend on the Mach number M_0 and the angle of incidence ϕ_v. Figures 6–8 show results for the cylinder with circular cross section for $k = 2.8$ and two Mach numbers ($M_0 = 0.4$ and 0.8). Inspection of these figures reveals that the boundary-layer refraction effects are small for $M_0 = 0.4$. For $\phi_v = 90$ deg (Fig. 6) the effects are even negligible, because the results of the calculations with and without boundary-layer flow coincide exactly. For the higher speed of $M_0 = 0.8$, however, the effects are significant, in particular for $\phi_v = 135$ and 153 deg as follows from Figs. 7 and 8. Furthermore, it is obvious that the refraction effects decrease when ϕ_v decreases. For values of ϕ_v less than 90 deg the effects are minimal for both $M_0 = 0.4$ and 0.8 because the waves propagate with the flow.

Application to an Aircraft Fuselage

The hybrid computational model is applied to investigate scattering and refractive effects of a fuselage of a Fokker 50-like aircraft that is geometrically modeled as an infinitely long cylinder with a noncircular cross section. The fuselage has been scaled down in such a way that the width equals two (in Fig. 1 $r_p = 1$ for $\theta_p = 0$ deg). The influence of the noncircular geometry and the influence of the velocity profile of a turbulent boundary layer on the acoustic pressure are assessed. The plane waves impinge on the cylinder (in Fig. 1 from the right-hand side) under different angles of incidence ϕ_v.

Two different phenomena are investigated: the influence of the velocity profile of a turbulent boundary layer and the influence of the noncircular geometry. First, the influence of the boundary layer is considered. For $M_0 = 0.8$ (corresponding to the cruise speed of a propfan-driven aircraft) the effects of the boundary-layer refraction on the acoustic surface pressure are shown in Figs. 9–11. When these results are compared with Figs. 6–8, it is observed that the boundary-layer refraction effects are of the same order of magnitude as for the cylinder with circular cross section. Inspection of Fig. 11 reveals that for $\phi_v = 153$ deg a maximum attenuation of sound pressure level of about 8 dB is reached.

In Figs. 12–16 the computed acoustic surface pressures on the cylinder with noncircular cross section are compared with the results of a cylinder with a circular cross section. For $M_0 = 0.4$ and $k = 2.8$ (corresponding to cruise conditions that are representative for the propeller-driven aircraft) the influence of the boundary-layer shear flow on the resultant noise is minimal, as can be observed

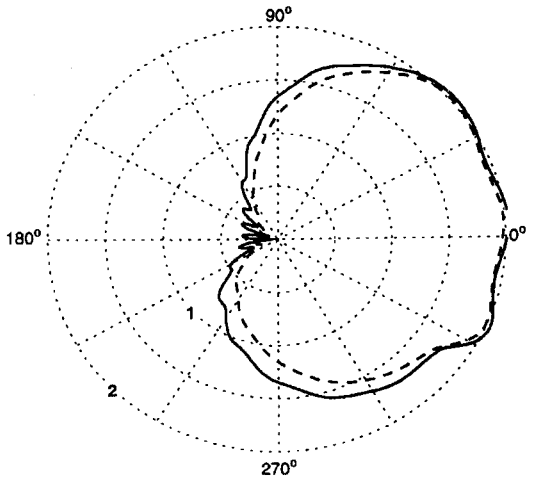

Fig. 9 Effects of the boundary-layer flow on the pressure distribution (amplitude) around the cylinder with a cross section similar to a Fokker 50 fuselage; $k = 5.6$, $M_0 = 0.8$, $\phi_v = 90$ deg: ——, Fokker 50 without boundary layer; and - - - -, Fokker 50 with boundary layer (turbulent velocity profile).

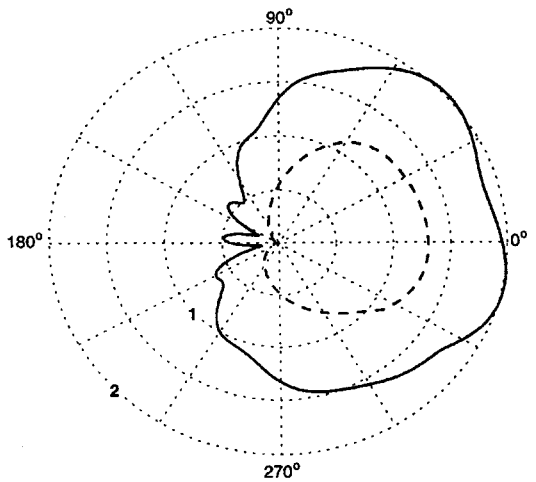

Fig. 10 Effects of the boundary layer flow on the pressure distribution (amplitude) around the cylinder with a cross section similar to a Fokker 50 fuselage; $k = 5.6$, $M_0 = 0.8$, $\phi_v = 135$ deg: ——, Fokker 50 without boundary layer; and - - - -, Fokker 50 with boundary layer (turbulent velocity profile).

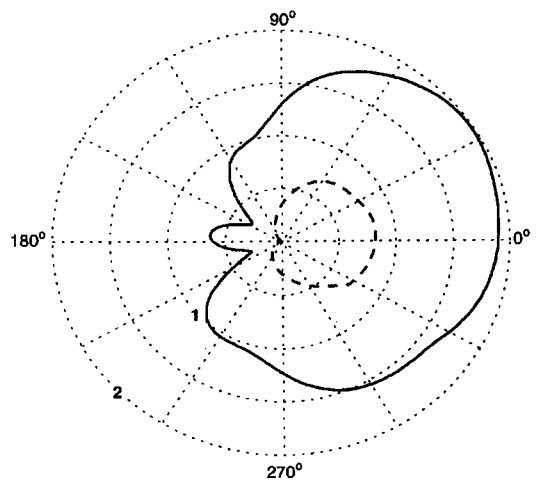

Fig. 11 Effects of the boundary-layer flow on the pressure distribution (amplitude) around the cylinder with a cross section similar to a Fokker 50 fuselage; $k = 5.6$, $M_0 = 0.8$, $\phi_v = 153$ deg: ——, Fokker 50 without boundary layer; - - - -, Fokker 50 with boundary layer (turbulent velocity profile).

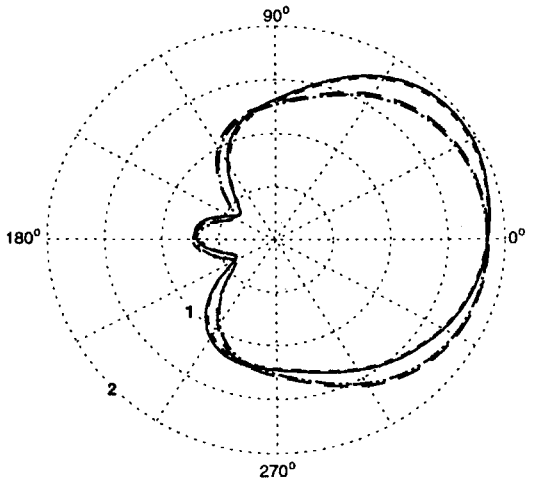

Fig. 12 Comparison of the pressure distribution (amplitude) around the cylinder with a cross section similar to a Fokker 50 fuselage and a circular cross section; $k = 2.8$, $M_0 = 0.4$, $\phi_v = 135$ deg: ——, Fokker 50 without boundary layer; and - - - -, Fokker 50 with boundary layer (turbulent velocity profile); – – –, circular without boundary layer; and ·—·—·, circular with boundary layer (turbulent velocity profile).

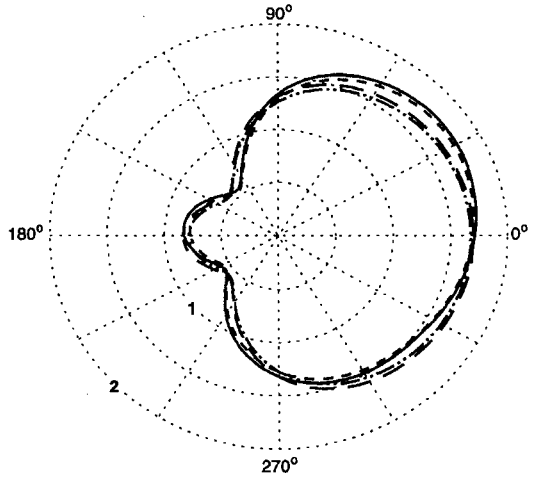

Fig. 13 Comparison of the pressure distribution (amplitude) around the cylinder with a cross section similar to a Fokker 50 fuselage and a circular cross section; $k = 2.8$, $M_0 = 0.4$, $\phi_v = 153$ deg: ——, Fokker 50 without boundary layer; - - - -, Fokker 50 with boundary layer (turbulent velocity profile); – – –, circular without boundary layer; and ·—·—·, circular with boundary layer (turbulent velocity profile).

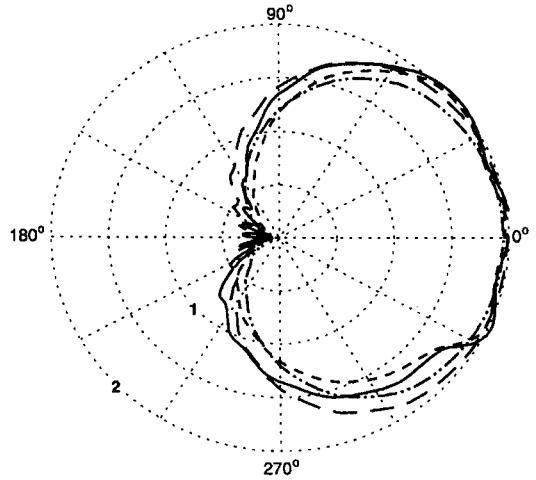

Fig. 14 Comparison of the pressure distribution (amplitude) around the cylinder with a cross section similar to a Fokker 50 fuselage and a circular cross section; $k = 5.6$, $M_0 = 0.8$, $\phi_v = 90$ deg: ——, Fokker 50 without boundary layer; - - - -, Fokker 50 with boundary layer (turbulent velocity profile); – – –, circular without boundary layer; and ·—·—·, circular with boundary layer (turbulent velocity profile).

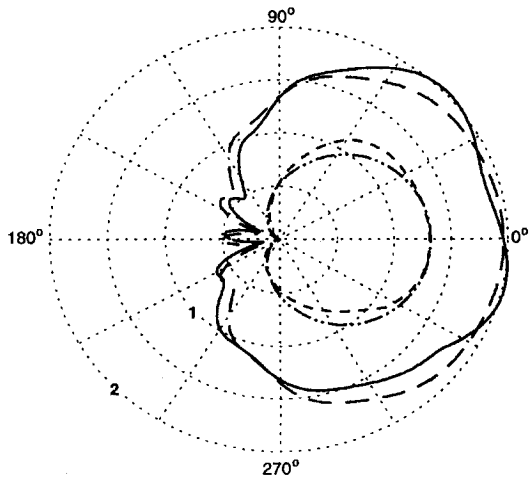

Fig. 15 Comparison of the pressure distribution (amplitude) around the cylinder with a cross section similar to a Fokker 50 fuselage and a circular cross section; $k = 5.6$, $M_0 = 0.8$, $\phi_v = 135$ deg: ——, Fokker 50 without boundary layer; - - - -, Fokker 50 with boundary layer (turbulent velocity profile); – – –, circular without boundary layer; and ·—·—·, circular with boundary layer (turbulent velocity profile).

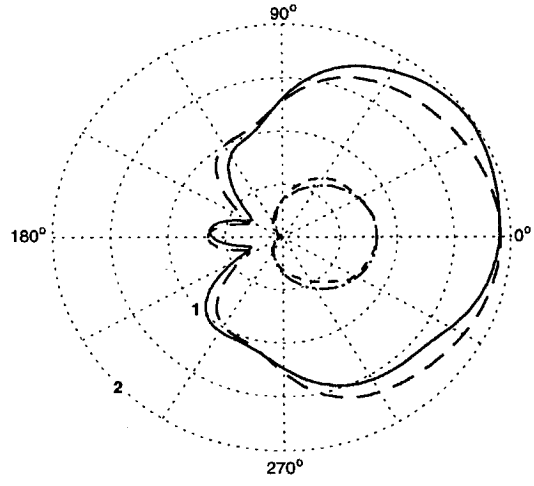

Fig. 16 Comparison of the pressure distribution (amplitude) around the cylinder with a cross section similar to a Fokker 50 fuselage and a circular cross section; $k = 5.6$, $M_0 = 0.8$, $\phi_v = 153$ deg: ——, Fokker 50 without boundary layer; - - - -, Fokker 50 with boundary layer (turbulent velocity profile); – – –, circular without boundary layer; and ·—·—·, circular with boundary layer (turbulent velocity profile).

from Figs. 12 and 13, where ϕ_v is 135 and 153 deg, respectively. It is obvious that for these conditions the effects of the noncircular geometry are larger than the effects of the boundary-layer refraction. When the results of the Fokker 50-like cross section are compared with the circular cross section, the maximum difference in sound pressure on the fuselage surface appears to be on the order of 1 dB of magnitude. For $M_0 = 0.8$ and $k = 5.6$ (corresponding to cruise conditions that are representative for the propfan-driven aircraft) the results are given in Figs. 14, 15, and 16, where ϕ_v is 90, 135, and 153 deg, respectively. Figures 14–16 show significant differences between the acoustic surface pressure at the Fokker 50-like cylinder and at the circular one. At the upper part (θ between 30 and 90 deg) the amplitude of the surface pressure at the Fokker 50-like cylinder is higher, whereas it is lower at the lower part (θ between 270 and 330 deg).

Conclusions and Recommendations

A hybrid computational model has been described that can compute the effects of sound propagation through a fuselage boundary layer. The fuselage has been represented by an infinitely long cylinder embedded in a longitudinal flow. For a specified boundary-layer velocity profile, the computational model calculates the acoustic pressure using a combination of finite elements and boundary elements. The model can be applied to predict scattering and refractive effects of cylinders of arbitrary cross section.

Results have been presented for a cylinder with a noncircular cross section similar to a Fokker 50-like fuselage. The effects of the noncircular geometry and the effects of a turbulent boundary-layer velocity profile on the acoustic pressure have been assessed. When the results of the noncircular cylinder (modeling the Fokker 50 fuselage) are compared with the results of a circular cylinder, the maximum difference in sound pressure on the fuselage surface appears to be on the order of 1 dB of magnitude. The prediction of noise inside the fuselage depends on, among others, the acoustic surface pressure at the outer side of the fuselage. Therefore, it is a prerequisite to have available computational models that accurately predict the exterior acoustic field. As shown in Figs. 12–16, the accuracy of the acoustic pressure predictions at the outer surface requires a correct description of the noncircular geometry (in particular for ϕ_v from 90 to 135 deg, where, usually, the propeller or propfan noise is located) and a precise modeling of the boundary-layer shear flow.

The effects of the boundary-layer velocity profile on the acoustic surface pressure strongly depend on the Mach number M_0 of the uniform flow, the wave number k, and the angle of incidence ϕ_v of the incoming wave. For the conditions $M_0 = 0.4$ and $k = 2.8$, which are representative for a propeller-driven aircraft, it can be concluded that there is hardly any attenuation of the pressure on the cylinder surface, even for large angles of incidence. For these conditions the effects of the noncircular geometry are larger than the effects of the boundary-layer refraction. When the Mach number is increased to $M_0 = 0.8$ and the wave number to $k = 5.6$ (corresponding with conditions representative for a propfan-driven aircraft), however, the effect of the boundary-layer velocity profile becomes more pronounced. A reduction up to 8 dB can be observed because of refraction of acoustic rays in the boundary layer.

The results of the section on modeling of boundary-layer shear flow show that the boundary-layer refraction is dependent on the shape of the boundary-layer velocity profile. It has been concluded that the velocity profile should be modeled as accurately as possible when refraction of acoustic rays is an important factor, which occurs for angles of incidence larger than 90 deg. Then, acoustic waves bend away from the cylinder and, as a result, lower pressure amplitudes are found on the surface of the cylinder.

Further investigations should take into account more general incident (propeller) fields instead of plane waves. Then, a large range of wave numbers α in axial direction has to be taken into account. From Eqs. (6) and (8) it is obvious that the governing equation for the pressure P becomes singular for $M(r) = -k/\alpha$. Near the region of the singular points, Eq. (6) has to be regularized. For one fixed wave number α (corresponding to a propagating incident plane wave), it can be shown that Eq. (6) cannot become singular for subsonic Mach numbers.

Acknowledgments

Part of this research has been carried out in cooperation with the Department of Mechanical Engineering, University of Twente. The authors would like to thank H. Tijdeman (University of Twente) and P. Sijtsma (National Aerospace Laboratory NLR) for fruitful discussions. The authors are grateful to H. H. Brouwer (National Aerospace Laboratory NLR) for bringing the aeroacoustic problem to their attention.

References

[1]Morse, P. M., and Ingard, K. U., *Theoretical Acoustics*, Princeton Univ. Press, Princeton, NJ, 1986, pp. 400–404.

[2]McAninch, G. L., and Rawls, J. W., "Effects of Boundary Layer Refraction and Fuselage Scattering on Fuselage Surface Noise from Advanced Turboprop Propellers," AIAA Paper 84-0249, Jan. 1984.

[3]Hanson, D. B., and Magliozzi, B., "Propagation of Propeller Tone Noise Through a Fuselage Boundary Layer," *Journal of Aircraft*, Vol. 22, No. 1, 1985, pp. 63–70.

[4]Lu, H., "Fuselage Boundary Layer Effects on Sound Propagation and Scattering," AIAA Paper 89-1098, April 1989.

[5]Spence, P. L., "Effects of Fuselage Boundary Layer on Noise Propagation from Advanced Propellers," *Journal of Aircraft*, Vol. 29, No. 6, 1992, pp. 1005–1011.

[6]Costabel, M., Ervin, V. J., and Stephan, E. P., "Experimental Convergence Rates for Various Couplings of Boundary and Finite Elements," *Mathematical Computer Modelling*, Vol. 15, Nos. 3–5, 1991, pp. 93–102.

[7]Goldstein, M. E., *Aeroacoustics*, McGraw–Hill, New York, 1976, pp. 2–10.

[8]Schenk, H. A., "Improved Integral Formulations for Acoustic Radiation Problems," *Journal of the Acoustical Society of America*, Vol. 44, No. 1, 1968, pp. 41–58.

[9]Wensing, J. A., "Computation of the Acoustic Field Around an Aircraft Fuselage," National Aerospace Lab. NLR, NLR TR 94235 L, Amsterdam, The Netherlands, June 1994.

[10]Lewis, J. G., "Algorithm 582: The Gibbs–Poole–Stockmeyer and Gibbs–King Algorithms for Reordering Sparse Matrices," *Association for Computing Machinery Transactions on Mathematical Software*, Vol. 8, No. 2, 1982, pp. 190–194.

[11]Schippers, H., and Wensing, J. A., "Coupling of Boundary and Finite Elements in Aeroacoustic Calculations," *Proceedings of the 11th GAMM-Seminar Kiel: Numerical Treatment of Coupled Systems, Notes on Numerical Fluid Mechanics*, Vol. 51, Vieweg–Verlag, Braunschweig, Germany, 1995, pp. 151–162 (NLR Rept. TP 95125 L).

[12]Schlichting, H., *Boundary-Layer Theory*, 7th ed., McGraw–Hill, New York, 1979, pp. 637, 638.